analytical chemistry

Article

Cite This: *Anal. Chem.* 2018, 90, 7510−7516

pubs.acs.org/ac

Evaluating Drug-Induced Liver Injury and Its Remission via Discrimination and Imaging of HClO and H_2S with a Two-Photon Fluorescent Probe

Xiaoyun Jiao,[†] Yongsheng Xiao,[†] Yong Li, Muwen Liang, Xilei Xie, Xu Wang,* and Bo Tang*

College of Chemistry, Chemical Engineering and Materials Science, Collaborative Innovation Center of Functionalized Probes for Chemical Imaging in Universities of Shandong, Key Laboratory of Molecular and Nano Probes, Ministry of Education, Institute of Molecular and Nano Science, Shandong Normal University, Jinan 250014, P. R. China

Supporting Information

ABSTRACT: Drug-induced liver injury (DILI) has aroused wide concern. Finding new markers or indicators as well as detoxification molecules for DILI is of great significance and good application prospect, which can help develop effective preclinical screening methodology and corresponding treatment protocols. Herein, in this article, DILI caused by antidepressant drugs of duloxetine and fluoxetine and its remission were evaluated by a two-photon fluorescent probe, **RPC-1**, through discriminating and imaging HClO and H_2S simultaneously. By being applied both in vitro and in vivo, **RPC-1** revealed slight up-regulation of HClO and negligible liver damage after administration of either of the two drugs. In contrast, an apparent up-regulation of HClO and obvious liver damage was observed after combined administration of the drugs. Meanwhile, the pretreatment of *N*-acetyl cysteine (NAC) resulted in the increasing of endogenous H_2S level, which contributed to the remission of DILI. The histological analysis and serological test both gave good consistency with the imaging results. These findings demonstrate that HClO may be an appropriate indicator of DILI, and H_2S plays an important role in the antidotal effect of NAC. We envision that **RPC-1** can be used as a powerful tool to predict clinical DILI and study the effect of antidote, as well as explore the molecular mechanisms involved.

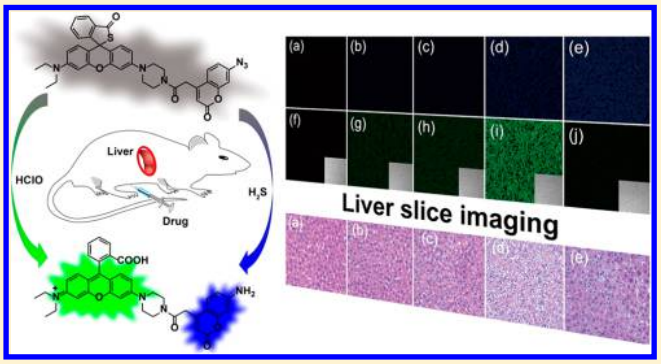

Drug-induced liver injury (DILI) has caused serious concern in public health issues. Moreover, it has become one of the most common considerations for a drug to be rejected from applications for a marketing license.[1,2] Since DILI is hard to predict, the preclinical screening methods for DILI are vital to reduce hepatotoxicity, improve patient safety, and raise therapeutic effect.[3,4] Fluorescence imaging is real-time, sensitive, and noninvasive[5−12] and has emerged as an efficient methodology for DILI testing.[13−15] Fluorescent probes specific for hepatotoxicity's biomarker imaging will contribute to the comprehensive understanding of pathogenesis and development of detoxification reagents.

HClO, one of the highly reactive oxygen species (hROS), is produced by myeloperoxidase (MPO)-mediated peroxidation of chloride ions[16] and is centrally linked to innate host defense, playing an important role in killing pathogens.[17] Meanwhile, the high oxidation ability of HClO makes it to be a double-edged sword that is harmful to organism, such as disabling mitochondria function of hepatocytes[18] or causing covalent cross-links between DNA and protein.[19] Although the up-regulation of HClO level in cancer cells upon anticarcinogen stimulation has been testified,[20] the fluctuation of HClO in liver tissue upon clinical drug challenge is much less clear. Considering the sensibility of HClO toward pathogens and foreign matters, we speculated that the drug metabolites may also initiate an up-regulation of endogenous HClO level, endowing HClO with good potential as an indicator for DILI prediction. Herein, a fluorescent probe specific for HClO can contribute to the validation of the above assumption.

In our previous work,[14] *N*-acetyl cysteine (NAC) was proved to be an antidote against DILI. But the mechanism of detoxification has not been studied in depth. It is well-known that NAC is the precursor of L-cysteine,[21] which is a substrate of cystathionine β-synthase (CBS) and cystathionine γ-lyase (CSE) to produce endogenous H_2S.[21,22] So NAC can be used as a H_2S promoter or stimulator.[23] Meanwhile, H_2S has shown protective or curative effects against organ injuries, including liver damage,[24] cardiac injury,[25] and kidney injury,[26] etc. Therefore, we speculated that H_2S, the metabolic product of NAC, may participate in the protection effect of NAC against drug-related organ injury. Therefore, a direct and reliable

Received: March 12, 2018
Accepted: May 21, 2018
Published: May 21, 2018

DOI: 10.1021/acs.analchem.8b01106
Anal. Chem. 2018, 90, 7510−7516

method that can visualize H_2S during drug challenge will give evidence of this issue.

To investigate the potential of HClO as an indicator for DILI and the H2S-mediated NAC antidotal effect, in this work, a new two-photon fluorescent probe, **RPC-1**, was designed and synthesized for the discrimination and imaging of HClO and H_2S simultaneously. **RPC-1** exhibits two emission bands corresponding to HClO and H_2S, respectively. Upon excitation with a two-photon laser, the presence of one or both of HClO/H_2S results in dramatic fluorescence enhancement within their own channels. Utilizing its outstanding features, **RPC-1** was successfully employed in exploring hepatotoxicity events caused by two antidepressant drugs, namely duloxetine and fluoxetine, both in vitro and in vivo. With the aid of **RPC-1**, we found that the incubation of either of these two drugs resulted in slight increase of HClO level and negligible liver damage. However, the combination drug pretreatment resulted in dramatic up-regulation of HClO, which was accompanied by obvious liver tissue injury. The remediation of liver damage was achieved by using NAC, which brought an apparent rise in H_2S level. These results demonstrate that HClO can be used as an indicator for DILI, and endogenous H_2S contributes greatly to the antidotal effect of NAC. It also reminds us of the risk of severe liver injury caused by the combination of antidepressant drugs, which should be avoided clinically.

EXPERIMENTAL SECTION

Materials. Unless otherwise stated, all reagents for synthesis were purchased from commercial suppliers and were used without further purification. *N*-Acetyl cysteine (NAC) was purchased from Aladdin Industrial Corporation (Shanghai). 3-(4,5-Dimethylthiazol-2-yl)-2,5-diphenyl tetrazolium bromide (MTT) was purchased from Sigma. Duloxetine and fluoxetine were obtained from Energy Chemical (Shanghai). The solvents were purified by conventional methods before use. Satorius ultrapure water (18 MΩ·cm) was used to prepare all aqueous solution. Silica gel (200−300 mesh) used for column chromatography was purchased from Qingdao Haiyang Chemical Co., Ltd. Test kits of alanine aminotransferase (ALT) and aspartate aminotransferase (AST) were purchased from Nanjing Jiancheng Bioengineering Institute. All the cells were purchased from the Cell Bank of the Chinese Academy of Science (Shanghai, China). Kunming mice (20 g) were purchased from the School of Medicine at Shandong University.

Instruments. ^{1}H NMR and ^{13}C NMR spectra were recorded on a Bruker Avance 400 spectrometer (Bruker Co., Ltd., Germany) with tetramethylsilane (TMS) as the internal standard. The mass spectra were obtained by Bruker maxis ultrahigh resolution-TOF MS spectrometer (Bruker Co., Ltd., Germany). Absorption spectra measurements were performed at room temperature on a UV-1700 UV−visible spectrophotometer (Shimadzu, Japan) with 1.0 cm quartz cells. Fluorescent spectra measurements were performed on FLS-980 Edinburgh fluorescence spectrometer (Edinburgh Instruments Ltd., England) with a xenon lamp and 1.0 cm quartz cuvettes at the slits of 2.0/2.0 nm. MTT assay was performed using a TRITURUS microplate reader. Fluorescence imaging of cells and mice was performed with the Zeiss LSM 880 NLO two-photon confocal laser scanning microscope (Zeiss, Germany) with an objective lens (×20).

Synthesis of RPC-1. The synthetic route of **RPC-1** is shown in Scheme S1.

Synthesis of Compound 1. The solution of 2-(4-diethylamino-2-hydroxy-benzoyl) benzoicacid (150 mg, 0.48 mmol) and *N*-(3-hydroxyphenyl)piperazine (85.3 mg, 0.48 mmol) in 5 mL of trifluoroacetic acid was heated at 90 °C for 12 h and then cooled to room temperature. The mixture was concentrated under vacuum and purified by column chromatography on silica gel (dichloromethane/methanol, 10:1 v/v) to afford compound **1** as a red solid (160 mg, 73%). ^{1}H NMR (400 MHz, DMSO-*d*6): δ 7.97 (d, J = 7.5 Hz, 1H), 7.77 (t, J = 8.6 Hz, 1H), 7.70 (t, J = 7.4 Hz 1H), 7.25 (d, J = 7.6 Hz, 1H), 6.68−6.72 (m, 2H), 6.49 (d, J = 8.7 Hz, 1H), 6.44 (q, J = 4.6 Hz 3H), 3.35 (q, J = 7.0 Hz, 4H), 3.12 (t, J = 5.3 Hz, 4H), 2.81 (t, J = 4.8 Hz, 4H), 1.09 (t, J = 7.0 Hz, 6H). ^{13}C NMR (100 MHz, DMSO-d6): δ 169.31, 153.60, 152.95, 152.60, 149.60, 135.85, 130.37, 129.09, 128.70, 127.07, 124.92, 124.53, 111.81, 108.81, 105.37, 101.21, 97.36, 84.67, 60.23, 48.91, 45.89, 44.26, 21.24, 14.56, 12.79. HRMS (ESI): calcd for $C_{28}H_{30}N_3O_3^+$ $[M]^+$= 456.2281, found 456.2291..

Synthesis of Compound 2. Compound **1** (160 mg, 0.35 mmol), 9-fluorenylmethyl chloroformate (130 mg, 0.5 mmol), and $NaHCO_3$ (125 mg, 1.5 mmol) were violently stirred in 10 mL of dry acetonitrile under nitrogen for 3 h at room temperature. After the solvent was removed under reduced pressure, the obtained dark red solid was dissolved in ethyl acetate for filtration. The filtrate was washed with H_2O and dried over anhydrous $MgSO_4$. Then, the solvent was removed under vacuum, and the residue was purified by silica gel column chromatography using petroleum ether/ethyl acetate (10:1, v/v) as eluent to obtain the product as dark red solid (210 mg, 88%). ^{1}H NMR (400 MHz, DMSO-*d*6): δ 7.99 (d, J = 7.5 Hz, 1H), 7.90 (d, J = 7.4 Hz, 2H), 7.78 (t, J = 6.4 Hz 1H), 7.71 (t, J = 7.3 Hz 1H), 7.64 (d, J = 7.4, 2H), 7.41 (t J = 7.2 Hz, 2H), 7.34 (t, J = 7.3 Hz, 2H), 7.25 (d, J = 7.6 Hz, 1H), 6.77 (s 1H), 6.71 (q, J = 6.5 Hz, 1H), 6.52 (d, J = 8.8 Hz, 1H), 6.42−6.48 (m, 3H), 4.42 (d, J = 6.4 Hz, 2H), 4.29 (t, J = 6.4, 1H), 3.44 (t, J = 6.5, 4H) 3.36 (q, J = 6.9, 4H),3.15 (t, J = 6.3 Hz, 4H), 1.09 (t, J = 6.9 Hz, 6H). ^{13}C NMR (100 MHz, DMSO-*d*6): δ 169.29, 154.76, 152.88, 152.68, 152.57, 149.62, 144.29, 141.26, 135.86, 130.40, 129.09, 128.85, 128.12, 127.60, 127.02, 125.46, 124.95, 124.50, 120.61, 112.29, 109.52, 108.91, 105.30, 101.94, 97.34, 84.47, 67.01, 60.22, 47.63, 47.27, 44.26, 21.23, 14.56, 12.79. HRMS (ESI): calcd for $C_{43}H_{40}N_3O_5^+$ $[M]^+$= 678.2962, found 678.2922.

Synthesis of Compound 3. To a stirred solution of compound **2** (210 mg, 0.31 mmol) in 1,2-dichloroethane (5 mL), 0.2 mL of phosphorus oxychloride was added dropwise, and the mixture was stirred for 4 h at 95 °C. After the solvent was removed under vacuum, the residue was dissolved in 5 mL of tetrahydrofuran and added dropwise into a solution containing thiocarbamide (76.0 mg, 1.0 mmol), triethylamine (1.0 mL), tetrahydrofuran (10.0 mL), and H_2O (100 μL). After being stirred overnight at room temperature, the solvent was removed under reduced pressure. The residue was dissolved with 50 mL of water and extracted with ethyl acetate. The organic layer was collected and dried over anhydrous sodium sulfate. After concentration, it was purified by silica gel column chromatography (petroleum ether/ethyl acetate, 5:1 v/v) to afford compound **3** as white solid (73 mg, 35%). ^{1}H NMR (400 MHz, DMSO-*d*6): δ 7.90 (d, J = 7.5 Hz, 2H), 7.83 (d, J = 7.2 Hz, 1H), 7.70 (t, J = 6.3 Hz 1H), 7.58−7.65 (m, 3H), 7.41 (t, J = 7.8, 2H), 7.34 (t J = 6.3 Hz, 2H), 7.17 (d, J = 7.7 Hz, 1H), 6.66 (d, J = 8.8 Hz, 3H), 6.61 (d, J = 4.1 Hz, 1H), 6.39 (q, J = 6.3 Hz, 1H), 6.32 (s, 1H), 4.41 (d, J = 6.5 Hz, 2H), 4.29 (t, J =

DOI: 10.1021/acs.analchem.8b01106
Anal. Chem. 2018, 90, 7510−7516

6.6 Hz, 1H), 3.43 (t, J = 6.8, 4H), 3.31 (q, J = 6.4, 4H),3.11 (t, J = 5.3 Hz, 4H), 1.08 (t, J = 6.9 Hz, 6H). ^{13}C NMR (100 MHz, DMSO-$d6$): δ 196.22, 157.52, 154.76, 152.00, 151.73, 148.69, 144.30, 141.27, 135.67, 135.02, 130.01, 129.81, 129.44, 128.14, 127.61, 125.47, 123.01, 120.63, 112.73, 112.32, 109.19, 107.75, 102.05, 97.35, 67.03, 62.43, 60.23, 47.73, 47.25, 44.18, 26.81, 21.24, 14.56, 12.86. HRMS (ESI): calcd for $C_{43}H_{39}N_3O_4S$ $[M + H]^+$ = 694.2734, found 694.2682.

Synthesis of Compound 4. Compound **3** (73 mg, 0.11 mmol) was dissolved in acetonitrile containing 15% piperidine and stirred for 30 min at room temperature. Then, the solvent was removed under vacuum, and the residue was purified by silica gel column chromatography using dichloromethane/methanol (20:1, v/v) as eluent to obtain the product as white solid (35 mg, 67%). ^{1}H NMR (400 MHz, DMSO-$d6$): δ 7.82 (d, J = 7.7 Hz, 1H), 7.68 (t, J = 7.6 Hz, 1H), 7.59 (t, J = 7.5 Hz, 1H), 7.16 (d, J = 7.7 Hz, 1H), 6.64 (s, 2H), 6.60 (t, J = 4.9 Hz, 2H), 6.38 (q, J = 7.6 Hz, 1H), 6.31 (d, J = 4.7 Hz, 1H), 3.31 (q, J = 8.0 Hz, 4H), 3.09 (t, J = 6.4 Hz, 4H), 2.81 (t, J = 5.3 Hz, 4H), 1.07 (t, J = 6.8 Hz, 6H). ^{13}C NMR (100 MHz, DMSO-$d6$): δ 196.16, 157.46, 151.95, 151.75, 151.06, 148.70, 135.71, 134.99, 130.03, 129.98, 129.49, 127.67, 123.05, 112.99, 112.67, 109.25, 107.66, 102.40, 97.28, 62.27, 45.25, 44.19, 42.97, 12.85. HRMS (ESI): calcd for $C_{28}H_{29}N_3O_2S$ $[M + H]^+$ = 472.2053, found 472.2058.

Synthesis of Compound RPC-1. A mixture of compound **5** (24.5 mg, 0.1 mmol) and EDC·HCl (19.2 mg, 0.1 mmol) was stirred in dry dichloromethane (3 mL) for 30 min at room temperature. Then, compound **4** dissolved in 2 mL of dry dichloromethane was added. After that, 4-dimethylaminopyridine (6.1 mg, 0.05 mmol) was added and stirred for 6 h at room temperature. The solvent was removed under reduced pressure, and the residue was purified by silica gel column chromatography (petroleum ether/ethyl acetate, 2:1 v/v) to afford probe **RPC-1** as yellowish white solid (10.5 mg, 15%). ^{1}H NMR (400 MHz, DMSO-$d6$): δ 7.83 (d, J = 7.9 Hz, 1H), 7.71 (d, J = 4.1 Hz, 1H), 7.68 (d, J = 4.8 Hz, 1H), 7.61 (t, J = 8.0 Hz, 1H), 7.17 (t, J = 4.0, 2H), 7.11 (q J = 6.4 Hz, 1H), 6.68−7.13 (m, J = 8.4 Hz, 3H), 6.62 (d, J = 7.9 Hz, 1H), 6.40 (q, J = 4.1 Hz, 1H), 6.33 (t, J = 6.6 Hz, 2H), 4.08 (s, 2H), 3.72 (t, J = 4.1 Hz, 2H), 3.61 (t, J = 4.0 Hz, 2H), 3.30−3.33 (m, J = 4.4 Hz, 6H), 3.22 (t, J = 4.3 Hz, 2H), 1.08 (t, J = 4.0 Hz, 6H). ^{13}C NMR (100 MHz, DMSO-$d6$): δ 196.21, 170.80, 167.19, 159.98, 157.52, 154.52, 151.62, 148.68, 143.64, 135.65, 135.01, 130.00, 129.43, 128.01, 127.65, 123.00, 117.06, 115.99, 115.20, 112.50, 112.22, 109.18, 107.74, 107.26, 101.88, 97.34, 62.44, 60.22, 48.02, 47.65, 45.32, 44.18, 41.42, 36.52, 21.23, 14.55, 12.85. HRMS (ESI): calcd for $C_{39}H_{34}N_6O_5S$ $[M + H]^+$ = 699.2384, $[M + Na]^+$ = 721.2203, found 699.2395, 721.2212.

RESULTS AND DISCUSSION

Design and Synthesis of RPC-1. In the recent years, the development of single fluorophore-based probes for HClO (thio-spiro ring opening[27−29]) or H_2S (reduction of azide to amine[30−35]), as well as the reversible sensing of HClO/H_2S pair (selenide and selenoxide interconverison[36,37]), have helped a lot for the deep understanding of HClO or H_2S biofunctions. However, the indistinguishable emission limited their further application. Utilizing a mixed solution of two different probes may be a choice. But some drawbacks still exist, such as different subcellular distribution and metabolic pathway of different probes, mutual interference in measurement, and more disturbance on organism, etc. Fortunately, the dual fluorophore-based probes with dual reaction sites have paved a way for the imaging of two closely related substances in living cells.[38−42]

The suitable fluorophores for fabricating such a probe should possess high quantum yield and distinguishable emission, as well as good specificity toward one specie only. Therefore, we chose 7-amino coumarin and rhodamine B, which are linked by a rigid piperazine, to constitute the skeleton. 7-Amino coumarin moiety is featured with an excitation maximum at 360 nm and an emission maximum at 445 nm. Rhodamine B moiety is characterized with an excitation maximum at 545 nm and an emission maximum at 580 nm. Moreover, rhodamine B can be also excited by 360 nm, paving the way for a dual-response two-photon probe with single excitation. Then we selected thiolactone[27−29] and azido[30−35] specific for HClO and H_2S to mask rhodamine B and 7-amino coumarin, respectively, to obtain **RPC-1** (detailed synthesis route, see Scheme S1). The spirocyclization of rhodamine B and azidation of 7-amino coumarin give low fluorescence background, which will recover dramatically in the presence of HClO or H_2S, guaranteeing good sensitivity in biological system (Scheme 1).

Scheme 1. Chemical Structure of RPC-1 and the Proposed Dual-Detection Mechanism

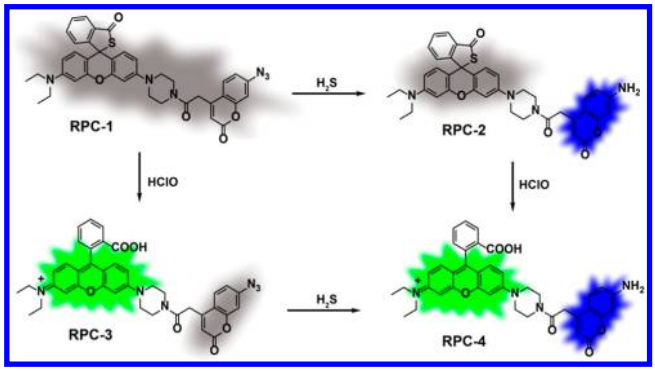

Spectral Response of RPC-1 to HClO and H_2S. The spectral response of **RPC-1** to HClO and H_2S was first investigated. The absorption spectra of **RPC-1** (Figure S1) gave maximum absorbance at 360 and 545 nm in the presence of H_2S and HClO, respectively, which correspond to the absorption spectra of 7-amino coumarin and rhodamine B. When H_2S and HClO were added simultaneously, the absorbance at 360 and 545 nm both increased, indicating the formation of RPC-4. Then the fluorescence spectra were investigated (Figure 1). As can be seen, upon incubation with different concentrations (0−100 μM) of H_2S, the gradual fluorescence enhancement (emission maximum at 445 nm with 360 nm excitation) of **RPC-1** was observed (Figure 1a). The fluorescence intensity exhibited a good linear (R^2 = 0.9901) response to H_2S, and the LOD ($3S_0/K$) was estimated to be 192.1 nM (Figure 1a inset). Meanwhile, the fluorescence of **RPC-1** (emission maximum at 580 nm with 545 nm excitation) increased with increasing HClO concentration in the range of 0−100 μM (Figure 1b), displaying a linear relationship (R^2 = 0.9913) and a LOD of 19.8 nM (Figure 1b inset). This resulted from the D−π−A structure recovering induced through the reduction of azido by H_2S[31,32] and the ring opening initiated by HClO.[27−29] Then the whole emission spectra of **RPC-1** were obtained after adding H_2S and HClO successively. As can be

DOI: 10.1021/acs.analchem.8b01106
Anal. Chem. 2018, 90, 7510−7516

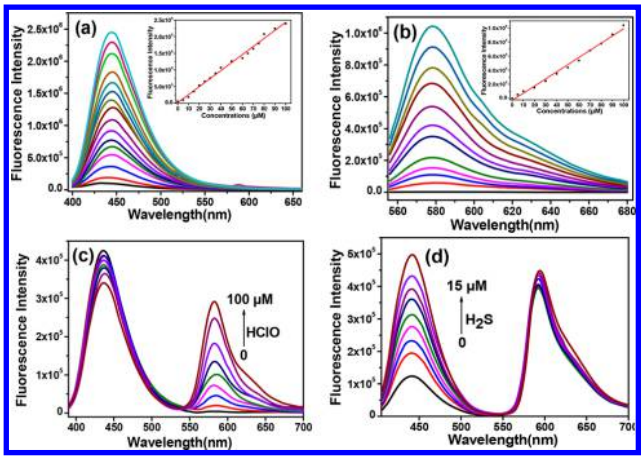

Figure 1. Fluorescence response of **RPC-1** (10 μM) to H_2S and HClO in PBS buffer (50 mM, pH 7.4, DMF 10% v/v). (a) Response of **RPC-1** to H_2S (0−100 μM). $\lambda_{ex}/\lambda_{em}$ = 360/445 nm. Inset: linear equation. (b) Response of **RPC-1** to HClO (0−100 μM). $\lambda_{ex}/\lambda_{em}$ = 545/580 nm. Inset: linear equation. (c) Response of **RPC-1** to HClO (0−100 μM) in the presence of H_2S (15 μM) with 360 nm excitation. (d) Response of **RPC-1** to H_2S (0−15 μM) in the presence of HClO (100 μM) with 360 nm excitation. Slit width: 2 nm/2 nm.

seen in Figure 1c, after various concentrations of HClO were added to the H_2S-pretreated **RPC-1** solution, very weak dropping of fluorescence at 445 nm and gradual fluorescence increase at 580 nm were observed, meaning that the addition of HClO could hardly influence the response of **RPC-1** toward H_2S. Correspondingly, the addition of H_2S to the HClO-pretreated **RPC-1** solution also induced a gradual fluorescence increase at 445 nm and negligible fluorescence variation at 580 nm (Figure 1d), suggesting that H_2S could not interfere with the signal of HClO. Therefore, **RPC-1** showed good dual-response character with satisfied emission separation and single-wavelength excitability. The responses of **RPC-1** to HClO and H_2S were also investigated with two-photon excitation of 750 nm (Figure S2), suggesting that **RPC-1** was suitable for a two-photon platform. The pH investigation (Figure S3) showed that **RPC-1** could work well in a physiological environment pH range.

Identification of the Reaction Mechanism. The reaction mechanism of **RPC-1** with H_2S and HClO was explored and identified by high-resolution mass spectrometer analysis (Figure S4). Upon the incubation of **RPC-1** with H_2S, the reaction mixture was found to have a mass peak at m/z 695.2280 (Figure S4a), corresponding to **RPC-2** as shown in Scheme 1. The solution of probe with HClO gave a mass peak at m/z 683.2589 (Figure S4b), corresponding to **RPC-3** as shown in Scheme 1. The results forcefully support the reaction-activated fluorescence turn-on mechanism illustrated in Scheme 1.

Kinetic Investigation of RPC-1. The kinetic profiles of **RPC-1** were investigated (Figure S5). In the absence of H_2S and HClO, the constant and low fluorescence intensity indicated that **RPC-1** was low background and stable toward light irradiation (line 1 in Figure S5a and Figure S5b). In the presence of H_2S, the fluorescence gradually increased and reached a plateau at about 900 s and then leveled off (Figure S5a, line 2). The addition of HClO induced a rapid and drastic fluorescence enhancement within seconds (Figure S5b, line 2). This significantly faster reaction of **RPC-1** toward HClO than H_2S contributes to the accurate dual-detection like the situation shown in Figure 1d.

The Specificity Investigation. The specificity of **RPC-1** toward H_2S and HClO was explored. As illustrated in Figure S6, no obvious fluorescence intensity change was triggered after incubation of **RPC-1** with a panel of intracellular substances except H_2S and HClO, guaranteeing the accuracy of simultaneous discrimination and detection of H_2S and HClO through dual-channel mode.

Visualizing H_2S and HClO in Live Cells. The feasibility of **RPC-1** for mapping H_2S and HClO level in biological system was assessed. MTT assay suggested that **RPC-1** possessed good biocompatibility (IC50 = 162.1 μM, Figure S7). Then, the exogenous H_2S and HClO were imaged in HepG2 cells with two-photon excitation microscopy. As displayed in Figure S8, in the control group, negligible fluorescence signal was observed in both of the two channels. However, significant enhancement of intracellular fluorescence intensity was obtained upon adding H_2S and HClO, respectively. Moreover, the colocalization experiments were performed to show the advantage of **RPC-1.** The cells incubated with **RPC-1** gave a Pearson's colocalization coefficient of 0.9671 between the blue and green channels after adding both H_2S and HClO (Figure S9). However, the cells incubated with compound **4** and compound **5** separately gave a Pearson's colocalization coefficient of only 0.7075 with apparent dotted distribution of the dyes (Figure S10). The results confirmed that **RPC-1** could give more reliable and accurate information relative to the mixed usage of two different probes.

Subsequently, the endogenously generated H_2S and HClO in RAW264.7 cells were imaged by **RPC-1.** First, NAC, a H_2S promotor,[23] was incubated with the cells. As can be seen in Figure 2 and Figure S11, after treatment of NAC, stronger

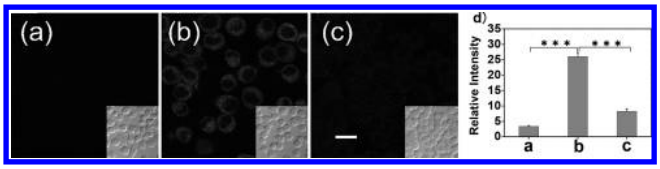

Figure 2. TPM imaging of endogenous H_2S in RAW264.7 cells. (a) Cells stained with **RPC-1** (10 μM, 60 min). (b) Cells were exposed to NAC (1.0 mM, 12 h) and then incubated with **RPC-1** (10 μM, 60 min). (c) Cells were exposed to NAC (1.0 mM) and PPG (50.0 mg/L) for 12 h and then incubated with **RPC-1** (10 μM, 60 min). (d) Relative fluorescence intensity of (a), (b), and (c). The images were obtained with 750 nm excitation and 400−500 nm collection. Values are the mean ± s.d. for n = 3, ***p < 0.001. Scale bar = 20 μm.

fluorescence signal in cells was observed than in the control group, meaning up-regulation of intracellular H_2S level induced by NAC. The increased fluorescence could be effectively attenuated by DL-propargylglycine (PPG), an inhibitor for CBS and CSE,[38] indicating good performance of **RPC-1** for endogenous H_2S detection. Also the role of NAC to raise H_2S level was further confirmed. Subsequently, endogenous HClO was stimulated by LPS and PMA,[43] and the images were captured (Figure 3 and Figure S12). As can be seen, apparent fluorescence enhancement was observed after stimulation, which declined after 4-aminobenzoic acid hydrazide (ABAH, an MPO inhibitor[44]) pretreatment. The endogenous H_2S and HClO in HepG2 cells were also imaged by **RPC-1** (Figures S13 and S14).

DOI: 10.1021/acs.analchem.8b01106
Anal. Chem. 2018, 90, 7510−7516

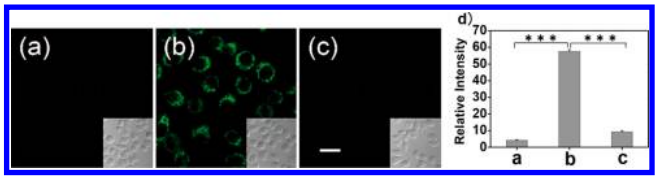

Figure 3. TPM imaging of endogenous HClO in RAW264.7 cells. (a) Cells stained with **RPC-1** (10 μM, 60 min). (b) Cells were exposed to LPS (1.0 μg/mL, 12h) and then incubated with PMA (1.0 μg/mL, 60 min), followed by treatment with **RPC-1** (10 μM, 60 min). (c) Cells were stained with ABAH (50.0 μM, 2h), and then successively treated with LPS (1.0 μg/mL, 12h) and PMA (1.0 μg/mL, 60 min), followed by treatment with **RPC-1** (10 μM, 60 min). (d) Relative fluorescence intensity of (a), (b), and (c). The images were obtained with 750 nm excitation and 550−650 nm collection. Values are the mean ± s.d. for n = 3, ***p < 0.001. Scale bar = 20 μm.

Visualizing H_2S and HClO in DILI Models. Encouraged by the good analytical features of **RPC-1** in both solution and live cells, we applied **RPC-1** to map the synergistic changes of H_2S and HClO level in DILI models. As is well-known, depression is a serious disorder, affecting 12−17% of the population at some point in life, resulting in major social and economic consequences.[45,46] To treat depression, antidepressant drugs are widely used. Although DILI induced by antidepressant drugs administration is frequent, the fact is that it is hard to predict. Therefore, exploring the possibility of HClO to be an indicator for DILI prediction appears to be very important. Fluoxetine and duloxetine are popular antidepressant drugs[47,48] and normally are taken long-term. They are metabolized by the same CYP450 isoenzymes.[49] However, the fact in reality is that few research studies on the liver injury of taking these two antidepressant drugs in combination has been reported.[49] Therefore, visualization of the liver damage with the aid of **RPC-1** at the cellular and tissue level may provide direct evidence on the understanding of nosogenesis and remission of DILI.

So the influence of fluoxetine and duloxetine challenge at a cellular level was first investigated by **RPC-1**. As presented in Figure 4, adding fluoxetine or duloxetine solely induced slight fluorescence enhancement in both the blue channel (400−500 nm, Figure 4b and 4c) and the green channel (550−650 nm, Figure 4h and 4i), indicating there was almost no up-regulation of HClO and H_2S under such a condition. In contrast, an apparent up-regulation of HClO was observed after combined administration (successively with a time interval of 2 h) of the two drugs (Figure 4j). Meanwhile, the endogenous H_2S level was correspondingly increased (Figure 4d). This indicated that the cells were more sensitive to the combined administration of the drugs. Then the effect of NAC was investigated. As can be seen, the fluorescence of green channel apparently declined (Figure 4k), and the signal of blue channel was even higher than that without NAC pretreatment (Figure 4e vs Figure 4d). The results showed that NAC pretreatment indeed increased the content of endogenous H_2S, and the HClO level was effectively depressed. When the cells were preincubated with PPG, the NAC-induced H_2S was suppressed (Figure 4f). Compared with Figure 4k, apparent increase of HClO level was reobserved (Figure 4l), confirming the antidotal role of H_2S. Similar results from HepG2 cells were obtained under the drug challenge (Figure S15).

Subsequently, the hepatotoxicity of fluoxetine and duloxetine was visualized at tissue level to deeply verify the toxicity

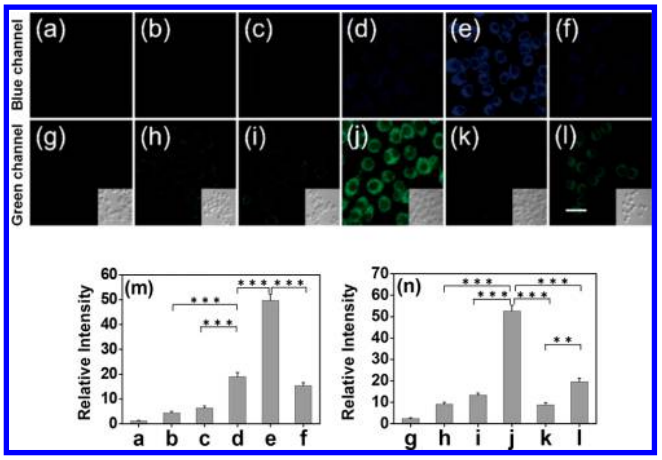

Figure 4. TPM imaging of endogenous H_2S and HClO in RAW264.7 cells upon drug treatment. (a) and (g) Cells stained with **RPC-1** (10 μM, 60 min). (b) and (h) Cells were exposed to fluoxetine (250 μM, 2h) and then incubated with **RPC-1** (10 μM, 60 min). (c) and (i) Cells were exposed to duloxetine (250 μM, 2h) and then incubated with **RPC-1** (10 μM, 60 min). (d) and (j) Cells were exposed to fluoxetine (250 μM, 2h) and then incubated with duloxetine (250 μM, 2h), followed by treatment with **RPC-1** (10 μM, 60 min). (e) and (k) Cells were exposed to NAC (1.0 mM, 1h) and then successively treated with fluoxetine (250 μM, 2h) and duloxetine (250 μM, 2h), followed by treatment with **RPC-1** (10 μM, 60 min). (f) and (l) Cells were exposed to PPG (50.0 mg/L, 2h) and NAC (1.0 mM, 1h) and then successively treated with fluoxetine (250 μM, 2h) and duloxetine (250 μM, 2h), followed by treatment with **RPC-1** (10 μM, 60 min). (m) and (n) Relative fluorescence intensity of (a)−(f) and (g)−(l). The images were obtained with 750 nm excitation and 400−500 nm (a−f) and 550−650 nm (g−l) collection, respectively. Values are the mean ± s.d. for n = 3, ***p < 0.001. Scale bar = 20 μm.

mechanism. Generally, Kunming mice were divided into five groups. As the control group, the first group was processed with an intraperitoneal injection of PBS buffer before a tail-vein injection of **RPC-1.** The second and third groups were given an intraperitoneal injection of PBS buffer solution containing fluoxetine or duloxetine and then a tail-vein injection of **RPC-1** 2 h later. The fourth group was processed first with an intraperitoneal injection of fluoxetine, followed by injection of duloxetine, and then **RPC-1**. The last group was pretreated with an intraperitoneal injection of NAC for 2 h before drug and probe administration. Then all the mice were anesthetized and dissected to isolate the livers, which were cut into slices for TPM fluorescence imaging. As shown in Figure 5, low fluorescence intensity was obtained in mice liver tissue in the control group, implying low HClO and H_2S level under normal conditions (Figure 5a and 5f). Similar to the results in cells, the addition of either of fluoxetine or duloxetine induced slight fluorescence enhancement in both the blue channel (Figure 5b and 5c) and the green channel (Figure 5g and 5h). By contrast, after administration of both fluoxetine and duloxetine, the mice liver in the fourth group emitted obvious fluorescence in the blue channel and green channel, indicating up-regulated H_2S and HClO after combined treatment by the drugs. Meanwhile, for the mice pretreated with NAC before drug administration, negligible fluorescence signal change was observed in the green channel, accompanied by a higher signal in the blue channel, meaning down-regulation of HClO and corresponding H_2S increase through NAC promotion. The results from tissue imaging confirmed the protection-mediated role of H_2S during the NAC treatment and verified that combined administration

DOI: 10.1021/acs.analchem.8b01106
Anal. Chem. 2018, 90, 7510−7516

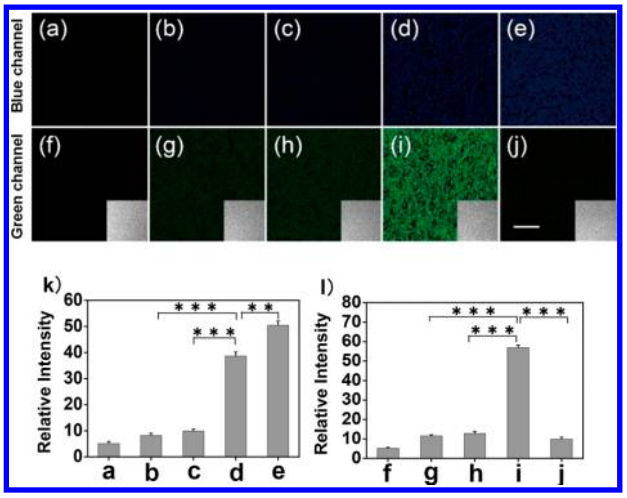

Figure 5. TPM images of rat liver slices. The mice were injected intraperitoneally with various substances and then injected with **RPC-1** (100 μM, 200 μL) via tail vein. (a) and (f) PBS buffer only as control group. (b) and (g) Fluoxetine (100 mg/kg, 2 h). (c) and (h): Duloxetine (100 mg/kg, 2 h). (d) and (i): Fluoxetine (100 mg/kg, 2 h) and then duloxetine (100 mg/kg, 2 h). (e) and (j): NAC (500 mg/kg, 1 h) and then fluoxetine (100 mg/kg, 2 h), followed by duloxetine (100 mg/kg, 2 h). (k) and (l) Relative fluorescence intensity of (a)−(e) and (f)−(j). The images were obtained with 750 nm excitation and 400−500 nm (a)−(e) and 550−650 nm (f)−(j) collection, respectively. Values are the mean ± s.d. for n = 3, $^{**}p < 0.01$, $^{***}p < 0.001$. Scale bar = 50 μm.

of fluoxetine and duloxetine could induce hepatotoxicity via up-regulation of HClO.

Next, the histological analysis on liver tissues was carried out to identify histological changes during drug administration. Briefly, Kunming mice liver sections were prepared from five groups processed with various conditions, including PBS buffer only, one drug administration, combined drug administration, and NAC pretreatment (Figure 6). As can be seen in Figure 6d,

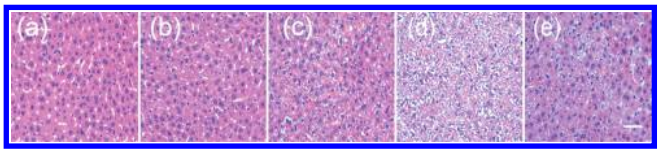

Figure 6. Representative H&E staining images of the liver of mice treated with various conditions. (a) PBS buffer only as control group. (b) Fluoxetine (100 mg/kg). (c) Duloxetine (100 mg/kg). (d) Fluoxetine (100 mg/kg) and duloxetine (100 mg/kg). (e) NAC (500 mg/kg) and then fluoxetine (100 mg/kg), followed by duloxetine (100 mg/kg). Scale bar = 20 μm.

compared with only one drug administration (Figure 6b and 6c), the obvious histological changes, including rupture of cell membrane, cellular shrinkage or blebbing, and condensation of chromatin, could be observed after combined drug administration, implying liver injury. The mice in NAC pretreatment group (Figure 6e) displayed no distinct changes in histological analysis, indicating that the liver injury could be effectively suppressed by NAC. Taken together, these results were in good agreement with the observation of in vitro fluorescent imaging using HClO as an indicator and H_2S for remission (Figure 4 and Figure 5). Since CYP450 enzyme system is responsible for phase I oxidative reactions,[50] we inferred that both fluoxetine and duloxetine, which target CYP450 enzyme, can inhibit or alter CYP450 enzyme activity, thus affecting the concentrations of the drugs or their metabolites, which brings liver injury. Meanwhile, the organism's self-protection mechanism was activated to up-regulate H_2S level, which can be promoted by adding NAC.

Serum concentrations of alanine aminotransferase (ALT) and aspartate aminotransferase (AST) are the most commonly used variables for assessment of liver damage.[51,52] Using the commercial test kits, the activities of ALT and AST in model mice were analyzed. As can be seen in Figure 7, compared with

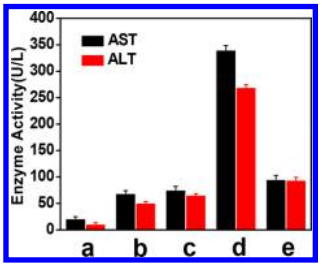

Figure 7. Activities of AST and ALT in mice serum treated with various conditions. (a) PBS buffer only as control group. (b) Fluoxetine (100 mg/kg). (c) Duloxetine (100 mg/kg). (d) Fluoxetine (100 mg/kg) and duloxetine (100 mg/kg). (e) NAC (500 mg/kg) and then fluoxetine (100 mg/kg), followed by duloxetine (100 mg/kg). Values are the mean ± s.d. for n = 3.

the control (Figure 7a), treatment of fluoxetine or duloxetine induced a mild increase of enzyme activity (Figure 7b and 7c). However, combined treatment of the two drugs resulted in a strong increase of enzyme activity (Figure 7d), indicating occurrence of severe liver injury. After pretreatment of NAC, the enzyme activity decreased and approximated the value of the single drug group (Figure 7e), displaying the remission effect of NAC. The enzyme activity test further confirmed the conclusions from cell and tissue analysis which used HClO as a DILI indicator.

Finally, drug-induced hepatotoxicity and H_2S generation and remission were monitored in vivo through a real-time way. As can be seen from Figure S16, after only one drug administration, the fluorescence of mice liver displayed negligible variation in both channels. Combined drug administration induced relatively obvious fluorescence enhancement in both channels, giving evidence of the up-regulation of both H_2S and HClO. Moreover, no obvious intensity augment in green channel was observed in NAC pretreatment group, which was accompanied by fluorescence increase in blue channel, showing suppression of HClO and increase of H_2S through NAC promotion. Both in vitro and in vivo results revealed for the first time the early warning potential of HClO for DILI and H_2S-mediated remission effect of NAC.

CONCLUSION

In conclusion, a new two-photon fluorescent probe, **RPC-1**, for the simultaneous discrimination and imaging of H_2S and HClO has been constructed. With the excellent properties of **RPC-1**, HClO as an efficient indicator for antidepressant-induced hepatotoxicity was exploited and verified. The synergetic variation of HClO and H_2S level gave evidence of the protection role of endogenous H_2S, which can be promoted by NAC. We envision that **RPC-1** may be employed as a powerful tool to predetect drug-induced liver injury and explore the molecular mechanism associated with H_2S protection.

DOI: 10.1021/acs.analchem.8b01106
Anal. Chem. 2018, 90, 7510−7516

■ ASSOCIATED CONTENT

Supporting Information

The Supporting Information is available free of charge on the ACS Publications website at DOI: 10.1021/acs.analchem.8b01106.

Experimental details, synthetic route, mass spectra, figures, imaging photos, and NMR spectra (PDF)

■ AUTHOR INFORMATION

Corresponding Authors

*E-mail: tangb@sdnu.edu.cn.

*E-mail: wangxu@sdnu.edu.cn.

ORCID

Bo Tang: 0000-0002-8712-7025

Author Contributions

†These authors contributed equally to this work.

Notes

The authors declare no competing financial interest.

■ ACKNOWLEDGMENTS

This work was supported by the National Natural Science Foundation of China (21390411, 21535004, 91753111, 21775093, and 21505088).

■ REFERENCES

(1) Nasr, A.; Lauterio, T. J.; Davis, M. W. *Adv. Ther.* **2011**, *28*, 842−856.

(2) Chen, M.; Vijay, V.; Shi, Q.; Liu, Z.; Fang, H.; Tong, W. *Drug Discovery Today* **2011**, *16*, 697−703.

(3) Sakatis, M.; et al. *Chem. Res. Toxicol.* **2012**, *25*, 2067−2082.

(4) Dimasi, J. *Clin. Pharmacol. Ther.* **2001**, *69*, 297−307.

(5) Jiao, X.; Li, Y.; Niu, J.; Xie, X.; Wang, X.; Tang, B. *Anal. Chem.* **2018**, *90*, 533−555.

(6) Xie, X.; Tang, F.; Shangguan, X.; Che, S.; Niu, J.; Xiao, Y.; Wang, X.; Tang, B. *Chem. Commun.* **2017**, *53*, 6520−6523.

(7) Niu, J.; Fan, J.; Wang, X.; Xiao, Y.; Xie, X.; Jiao, X.; Sun, C.; Tang, B. *Anal. Chem.* **2017**, *89*, 7210−7215.

(8) Xie, X.; Li, M.; Tang, F.; Li, Y.; Zhang, L.; Jiao, X.; Wang, X.; Tang, B. *Anal. Chem.* **2017**, *89*, 3015−3020.

(9) Li, Y.; Wang, X.; Yang, J.; Xie, X.; Li, M.; Niu, J.; Tong, L.; Tang, B. *Anal. Chem.* **2016**, *88*, 11154−11159.

(10) Xie, X.; Yang, X.; Wu, T.; Li, Y.; Li, M.; Tan, Q.; Wang, X.; Tang, B. *Anal. Chem.* **2016**, *88*, 8019−8025.

(11) Wang, X.; Lv, J.; Yao, X.; Li, Y.; Huang, F.; Li, M.; Yang, J.; Ruan, X.; Tang, B. *Chem. Commun.* **2014**, *50*, 15439−15442.

(12) Wang, X.; Sun, J.; Zhang, W.; Ma, X.; Lv, J.; Tang, B. *Chem. Sci.* **2013**, *4*, 2551−2556.

(13) Shuhendler, A.; Pu, K.; Cui, L.; Uetrecht, J.; Rao, J. *Nat. Biotechnol.* **2014**, *32*, 373−380.

(14) Li, Y.; Xie, X.; Yang, X.; Li, M.; Jiao, X.; Sun, Y.; Wang, X.; Tang, B. *Chem. Sci.* **2017**, *8*, 4006−4011.

(15) Cheng, D.; Xu, W.; Yuan, L.; Zhang, X. *Anal. Chem.* **2017**, *89*, 7693−7700.

(16) Pattison, D.; Davies, M. *Biochemistry* **2006**, *45*, 8152−8162.

(17) Prokopowicz, Z.; Arce, F.; Biedron, R.; Chiang, C.; Ciszek, M.; Katz, D.; Nowakowska, M.; Zapotoczny, S.; Marcinkiewicz, J.; Chain, B. *J. Immunol.* **2010**, *184*, 824−835.

(18) Jaeschke, H. *Am. J. Physiol-Gastr. L.* **2006**, *290*, 1083−1088.

(19) Kulcharyk, P. A.; Heinecke, J. *Biochemistry* **2001**, *40*, 3648−3656.

(20) Zhu, H.; Fan, J.; Wang, J.; Mu, H.; Peng, X. *J. Am. Chem. Soc.* **2014**, *136*, 12820−12823.

(21) Szabo, C. *Nat. Rev. Drug Discovery* **2007**, *6*, 917−935.

(22) Whiteman, M.; Le Trionnaire, S.; Chopra, M.; Fox, B.; Whatmore, J. *Clin. Sci.* **2011**, *121*, 459−488.

(23) Zanardo, R.; Brancaleone, V.; Distrutti, E.; Fiorucci, S.; Cirino, G.; Wallace, J. *FASEB J.* **2006**, *20*, 1411−1418.

(24) Tan, G.; Pan, S.; Li, J.; Dong, X.; Kang, K.; Zhao, M.; Jiang, X.; Kanwar, J.; Qiao, H.; Jiang, H.; Sun, X. *PLoS One* **2011**, *6*, e25943.

(25) Wang, X.; Yang, C.; Zheng, D.; Mo, L.; Lan, A.; Yang, Z.; Hu, F.; Chen, P.; Liao, X.; Feng, J. *Mol. Cell. Biochem.* **2012**, *363*, 419−426.

(26) Kasinath, B. *Kidney Int.* **2014**, *85*, 1255−1258.

(27) Ding, S.; Zhang, Q.; Xue, S.; Feng, G. *Analyst* **2015**, *140*, 4687−4693.

(28) Zhou, J.; Li, L.; Shi, W.; Gao, X.; Li, X.; Ma, H. *Chem. Sci.* **2015**, *6*, 4884−4888.

(29) Zhan, X.-Q.; Yan, J.-H.; Su, J.-H.; Wang, Y.-C.; He, J.; Wang, S.-Y.; Zheng, H.; Xu, J.-G. *Sens. Actuators, B* **2010**, *150*, 774−780.

(30) Lippert, A.; New, E.; Chang, C. *J. Am. Chem. Soc.* **2011**, *133*, 10078−10080.

(31) Mao, G.-J.; Wei, T.-T.; Wang, X.-X.; Huan, S.; Lu, D.-Q.; Zhang, J.; Zhang, X.-B.; Tan, W.; Shen, G.-L.; Yu, R.-Q. *Anal. Chem.* **2013**, *85*, 7875−7881.

(32) Chen, B.; Li, W.; Lv, C.; Zhao, M.; Jin, H.; Jin, H.; Du, J.; Zhang, L.; Tang, X. *Analyst* **2013**, *138*, 946−951.

(33) Bae, S. K.; Heo, C. H.; Choi, D. J.; Sen, D.; Joe, E.-H.; Cho, B. R.; Kim, H. M. *J. Am. Chem. Soc.* **2013**, *135*, 9915−9923.

(34) Yang, S.; Qi, Y.; Liu, C.; Wang, Y.; Zhao, Y.; Wang, L.; Li, J.; Tan, W.; Yang, R. *Anal. Chem.* **2014**, *86*, 7508−7515.

(35) Zhang, J.; Guo, W. *Chem. Commun.* **2014**, *50*, 4214−4217.

(36) Lou, Z.; Li, P.; Pan, Q.; Han, K. *Chem. Commun.* **2013**, *49*, 2445−2447.

(37) Wang, B.; Li, P.; Yu, F.; Song, P.; Sun, X.; Yang, S.; Lou, Z.; Han, K. *Chem. Commun.* **2013**, *49*, 1014−1016.

(38) Yi, L.; Wei, L.; Wang, R.; Zhang, C.; Zhang, J.; Tan, T.; Xi, Z. *Chem. - Eur. J.* **2015**, *21*, 15167−15172.

(39) Zhang, P.; Li, J.; Li, B.; Xu, J.; Zeng, F.; Lv, J.; Wu, S. *Chem. Commun.* **2015**, *51*, 4414−4416.

(40) Yuan, L.; Lin, W.; Xie, Y.; Chen, B.; Zhu, S. *J. Am. Chem. Soc.* **2012**, *134*, 1305−1315.

(41) Chen, W.; Pacheco, A.; Takano, Y.; Day, J.; Hanaoka, K.; Xian, M. *Angew. Chem., Int. Ed.* **2016**, *55*, 9993−9996.

(42) Ang, C. Y.; Tan, S. Y.; Wu, S.; Qu, Q.; Wong, M. F. E.; Luo, Z.; Li, P.-Z.; Selvan, S. T.; Zhao, Y. *J. Mater. Chem. C* **2016**, *4*, 2761−2774.

(43) Li, G.; Lin, Q.; Sun, L.; Feng, C.; Zhang, P.; Yu, B.; Chen, Y.; Wen, Y.; Wang, H.; Ji, L.; Chao, H. *Biomaterials* **2015**, *53*, 285−295.

(44) Hu, J.; Wong, N.; Gu, Q.; Bai, X.; Ye, S.; Yang, D. *Org. Lett.* **2014**, *16*, 3544−3547.

(45) Kessler, R.; McGonagle, K.; Zhao, S.; Nelson, C.; Hughes, M.; Eshleman, S.; Wittchen, H.; Kendler, K. *Arch. Gen. Psychiatry* **1994**, *51*, 8−19.

(46) Wong, M. L.; Licinio, J. *Nat. Rev. Neurosci.* **2001**, *2*, 343−351.

(47) Demirdaş, A.; Nazıroğlu, M.; Övey, İ. *Mol. Neurobiol.* **2017**, *54*, 4683−4695.

(48) Mun, A.; Lee, S.; Kim, G.; Kang, H.; Kim, J.; Kim, S. *Anticancer Res.* **2013**, *33*, 3691−3698.

(49) Voican, C. S.; Corruble, E.; Naveau, S.; Perlemuter, G. *Am. J. Psychiatry* **2014**, *171*, 404−415.

(50) Wille, S. M.; Cooreman, S. G.; Neels, H. M.; Lambert, W. E. *Crit. Rev. Clin. Lab. Sci.* **2008**, *45*, 25−89.

(51) Lee, I.; Liu, J.; Yang, K. *Am. J. Trop. Med. Hyg.* **2005**, *72*, 221−226.

(52) Holoman, J.; Glasa, J.; Galbavy, S.; Danis, D.; Molnarova, A.; Kazar, J.; Bednarova, A.; Misianik, J. *Bratisl Lek. Listy.* **2002**, *103*, 70−75.

DOI: 10.1021/acs.analchem.8b01106
Anal. Chem. 2018, 90, 7510−7516